Virulence

ISSN: 2150-5594 (Print) 2150-5608 (Online) Journal homepage: www.tandfonline.com/journals/kvir20

Crystal structure of the *Legionella pneumophila* effector SidL (Lpg0437) in complex with its metaeffector LegA11 (Lpg0436)

Dominik A. Machtens, Carissa A. Hutchison, Ashley M. Stein, Jan Eberhage, Jonas M. Willerding, Susanne Eschenburg, Stephanie R. Shames & Thomas F. Reubold

To cite this article: Dominik A. Machtens, Carissa A. Hutchison, Ashley M. Stein, Jan Eberhage, Jonas M. Willerding, Susanne Eschenburg, Stephanie R. Shames & Thomas F. Reubold (2026) Crystal structure of the *Legionella pneumophila* effector SidL (Lpg0437) in complex with its metaeffector LegA11 (Lpg0436), Virulence, 17:1, 2646775, DOI: 10.1080/21505594.2026.2646775

To link to this article: https://doi.org/10.1080/21505594.2026.2646775

VIRULENCE
2026, VOL. 17, NO. 1, 2646775
https://doi.org/10.1080/21505594.2026.2646775

Taylor & Francis
Taylor & Francis Group

BACTERIAL PATHOGENESIS

OPEN ACCESS Check for updates

Crystal structure of the *Legionella pneumophila* effector SidL (Lpg0437) in complex with its metaeffector LegA11 (Lpg0436)

Dominik A. Machtens [a§], Carissa A. Hutchison [b*], Ashley M. Stein [c*], Jan Eberhage [a,d], Jonas M. Willerding [a$], Susanne Eschenburg [a,d], Stephanie R. Shames [b*], and Thomas F. Reubold [a*]

[a]Institute for Biophysical Chemistry, Hannover Medical School, Hannover, Germany; [b]Department of Microbiology, Genetics, and Immunology, Michigan State University, East Lansing, MI, USA; [c]Division of Biology, Kansas State University, Manhattan, KS, USA; [d]Cluster of Excellence RESIST (EXC 2155), Hannover Medical School, Hannover, Germany

ABSTRACT

Legionella pneumophila is an opportunistic human pathogen that causes atypical pneumonia called Legionnaires' Disease. To replicate within host cells, *L. pneumophila* injects up to 330 effector proteins into the host cytosol via a Dot/Icm type IV secretion system. Several effectors, called metaeffectors, regulate the activity of other effectors within infected host cells through direct protein-protein interactions. LegA11 (AnkJ/Lpg0436) has been identified as a metaeffector of SidL (Ceg14/Lpg0437), one of eight *L. pneumophila* effectors that inhibit host mRNA translation. LegA11 binds and suppresses SidL enzymatic activity, but the molecular basis of this regulation and impact on mRNA translation are unknown. Here, we present the crystal structure of SidL in complex with LegA11 to a resolution of 2.4 Å, revealing a high-affinity 1:1 complex with an extensive interaction interface of ~ 2300 Å^2. Using isothermal titration calorimetry, we determined a dissociation constant of 1.8 nM. *In vitro* translation assays demonstrate that SidL inhibits mRNA translation, and this activity is completely suppressed by LegA11. Mutagenesis of key interface residues in LegA11 disrupts complex formation and abolishes its metaeffector activity, confirming that LegA11 regulates SidL through direct protein-protein interaction. These findings show that LegA11 is a metaeffector that contributes to suppression of host mRNA translation by *L. pneumophila*.

ARTICLE HISTORY
Received 19 November 2025
Revised 11 February 2026
Accepted 13 March 2026

KEYWORDS
Legionella pneumophila; effector; metaeffector; mRNA translation

Introduction

Legionella pneumophila is an opportunistic pathogen that is ubiquitous in freshwater environments where it parasitizes free-living amoebae [1]. *L. pneumophila* can also replicate within alveolar macrophages, leading to a potentially life-threatening atypical pneumonia called Legionnaires' Disease. To replicate within host cells, *L. pneumophila* remodels the phagosome into a replication-permissive endoplasmic reticulum-like compartment called the *Legionella*-containing vacuole (LCV). To achieve this, *L. pneumophila* injects up to 330 effector proteins into the cytosol of the host cell through a Dot/Icm type IV secretion system (T4SS) [2]. *L. pneumophila* effectors interfere with and subvert key host cellular processes including ubiquitin-dependent proteasomal degradation, cell death, phagocytosis, vesicular trafficking, autophagy, and mRNA translation [3].

Several cellular processes are targeted by multiple effectors, reflecting *L. pneumophila*'s co-evolution with phylogenetically diverse hosts [4]. So far, eight different effectors have been identified in *L. pneumophila* that inhibit host mRNA translation. Lgt1 (Lpg1368), Lgt2 (Lpg2862), and Lgt3 (Lpg1488) are glycosyl transferases that transfer a glucose moiety to a specific serine residue in the eukaryotic translation elongation factor 1A [5,6]. The serine/threonine kinase LegK4 (Lpg0208) blocks translation by phosphorylation of a threonine residue in Hsp70 proteins [7], whereas VipF (Lpg0103) is an acetyl transferase that targets eukaryotic initiation factor 3 complex [8]. SidI (Lpg2504) transfers a mannosyl group to several ribosomal proteins [9]. The mechanism of action of RavX (Lpg1489) is currently unknown. SidL (Ceg14/Lpg0437) blocks translation via an unknown mechanism but is known to bind actin and has recently been shown to function as an ATPase that hydrolyzes ATP to AMP and pyrophosphate in the presence of host actin [10,11]. The dedication of multiple effectors to subversion of host

CONTACT Stephanie R. Shames shames@msu.edu; Thomas F. Reubold reubold.thomas@mh-hannover.de
*Denotes equal contribution.
§Current address: Department of Gastroenterology, Hepatology, Infectious Diseases and Endocrinology, Hannover Medical School, Carl-Neuberg-Straße 1, Hannover 306,025, Germany.
$Current address: Department of Nephrology and Hypertension, Hannover Medical School, Carl-Neuberg-Straße 1, Hannover 306,025, Germany.
Supplemental data for this article can be accessed online at https://doi.org/10.1080/21505594.2026.2646775

translation machinery underscores its importance for *L. pneumophila* virulence.

Work over the past 15 years has shown that a subset of *L. pneumophila* effectors, termed metaeffectors, do not exclusively target host proteins but instead serve to regulate the function of other effectors through a direct protein-protein interaction [12,13], distinguishing them from antagonistic effectors that exert opposing biochemical activities on the same host factor(s) [13]. Both SidI and SidL are regulated by metaeffectors, suggesting a role for this regulatory mechanism in *L. pneumophila*'s subversion of host mRNA translation. SidI is regulated by MesI (Metaeffector of SidI), which forms a high-affinity 1:1 complex with SidI and fully suppresses SidI-mediated translation inhibition and toxicity [14,15]. The effector LegA11 (AnkJ/Lpg0437) binds SidL and alleviates the toxic effect of SidL in yeast cells [11,16], but the molecular and biophysical underpinnings of the SidL-LegA11 interaction and impact of LegA11 on SidL-mediated translation inhibition are unknown.

Here, we present the crystal structure of SidL in complex with its cognate metaeffector LegA11 to a resolution of 2.4 Å. Using an *in vitro* translation assay, we show that SidL inhibits mRNA translation by an order of magnitude and that this activity is suppressed in the presence of LegA11. Based on the crystal structure, we identified residues in LegA11 that upon mutation disrupt the binding interface and abolish the metaeffector activity of LegA11. Thus, LegA11 is a metaeffector that contributes to *L. pneumophila*'s subversion of host mRNA translation via a direct protein-protein interaction with its cognate effector, SidL [17].

Material and Methods

Bacterial strains, cell culture, and growth conditions

Escherichia coli strains used for cloning (Top10Invitrogen; DH5αλ*pir*; a gift from Dr. Craig Roy, Yale University) and protein expression [BL21 (DE3); Invitrogen] were grown at 37°C in lysogeny broth (LB) medium supplemented with antibiotics for plasmid selection [100 µg/mL ampicillin (GoldBio, A-301), 50 µg/mL kanamycin (GoldBio K-120), 25 µg/mL chloramphenicol (GoldBio, C-105)]. *L. pneumophila*SRS43 (Lp02 *thyA*+;a gift from Dr. Craig Roy, Yale University [18]) strains were cultured on charcoal N (2-acetamido)-2-aminoethanesulfonic acid (ACES)-buffered yeast extract [10 g/L ACES (Sigma, A9758), 10 g/L yeast extract (BD, 212,750), 2 g/L activated charcoal (Sigma, C5510), pH 6.9] freshly supplemented with filter sterilized L-cysteine (0.4 g/L; Sigma, C7352) and Fe $(NO_3)_3$ (0.135 g/L; Sigma, 216,828) at 37°C [19]. Liquid ACES-buffered yeast extract (AYE) was prepared as described without charcoal and agar. When necessary, media were supplemented with 10 µg/mL chloramphenicolfor plasmid selection. Plasmid-based gene expression in *L. pneumophila* was induced with 1 mM of filter sterilized isopropyl β-D-1-thiogalactopyranoside (IPTG; GoldBio, I2481C).

Acanthamoeba castellanii strain Neff was acquired from the American Type Culture Collection (ATCC #30010) and maintained in PYG broth [7.5 g/L proteose peptone (BD, 211,693), 7.5 g/L yeast extract (BD, 212,750, 15 g/LD(+)-glucose (Thermo, A1682836), 0.4 mM $CaCl_2$ (Sigma, C4901), 4 mM $MgSO_4$ (Sigma, M7506), 3.4 mM Na citrate (Sigma, W302600), 50 µM $F_3(NH_4)_2(SO_4)_2$, (Sigma, 215,406), 2.5 mM Na_2HPO_4 (Sigma, S9763), 2.5 mM KH_2PO_4 (Sigma, P5655), pH 6.5] at 25°C [20].

Molecular cloning and strain construction

Oligonucleotide primersequences are listed in Suppl. Table S1. For expression of His_6-Myc fusion proteins, the respective *L. pneumophila* genes were cloned into pT7HMT, a gift from Dr. Brian Geisbrecht [21]. Wild-type *sidL* and *legA11* were amplified from *L. pneumophila* SRS43 genomic DNA (gDNA) using SidLBamHI-F/SidLNotI-R and LegA11BamHI-F/LegA11NotI-R primer pairs. *legA11*$_{K195A/F239R/G240R/F243R}$ (*legA11*-4 M) was amplified from cDNA on a high copy cloning vector purchased from Twist Biosciences (San Francisco, CA) using LegA11BamHI-F/LegA11NotI-R. BamHI/NotI-digested fragments were purified and ligated into BamHI/NotI-digested pT7HMT [21]. Sequence-confirmed constructs (Genewiz) were transformed into chemically competent *E. coli* Top10 and BL21 (DE3) for maintenance and protein expression, respectively. For genetic complementation of Δ*sidL* and Δ*legA11* mutations, *sidL* and *legA11* were amplified from *L. pneumophila* SRS43 gDNA using SidLJBBamHI-F/SidLSalI-R and LegA11JBBamHI-F/LegA11SalI-R primer pairs and ligated as BamHI/SalI fragments into BamHI/SalI-digested pSN85, a gift from Dr. Craig Roy [22]. Sequence confirmed pSN85:*legA11* and pSN85:*sidL* plasmids were transformed into electrocompetent *L. pneumophila* Δ*legA11* and Δ*sidL* using a BioRad Gene Pulser (2400 V, 25 µF, 2 mm) [14].

L. pneumophila SRS43 Δ*legA11* and Δ*sidL* were generated by allelic exchange [18]. Deletion constructs were generated by cloning 5" and 3" flanking regions of each gene into pSR47S. To generate pSR47S:Δ*legA11*,

5" and 3" flanking regions were amplified using LegA11KO1-F/LegA11KO1-R and LegA11KO2-F/LegA11KO2-R primer pairs, digested with SacI/NotI and NotI/SalI, respectively, and ligated into SacI/SalI-digested pSR47S (a gift from Dr. Craig Roy). To generate pSR47S:Δ*sidL*, 5" and 3" flanking regions were amplified using SidLKO1-F/SidLKO1-R and SidLKO2-F/SidLKO2-R primer pairs, digested with SacI/NotI and NotI/SalI, respectively, and ligated into SacI/SalI-digested pSR47S. Ligation reactions were transformed into chemically competent *E. coli* DH5αλ*pir*. Deletion constructs were validated by colony PCR and Sanger Sequencing (Genewiz) and conjugated into *L. pneumophila* SRS43 followed by selection of sucrose-resistant, kanamycin-sensitive colonies were screened by PCR and Sanger sequencing to verify gene deletion [23].

Protein expression and purification

The coding sequences of *sidL* (*lpg0437*) (UniProt accession number Q5ZYD5) in full-length (SidL_1s_BamHI/SidL_666as_SalI) or in N- and C-terminally truncated form (SidL_23s_BamHI/SdiL_640as_SalI; SidL_76s_BamH/SidL_645as_SalI) and of *legA11*(*lpg0436*) in full-length (LegA11_1s_BamHI/LegA11_269as_SalI) were amplified from *Legionella pneumophila* strain Philadelphia 1 (DSM-7513, DSMZ, Braunschweig, Germany) gDNA using primer pairs and cloned into either pGEX-4T1-TEV or pMEX-4T1-TEV [24]. Point mutations were introduced by overlap-PCR. The correctness of the resulting constructs was verified by sequencing (Seqlab, Göttingen, Germany). The constructs were expressed in *Escherichia coli* BL21 (DE3) cells grown to an OD of 1.0 in terrific broth. Expression was induced with 0.2 mM IPTG (Thermo Scientific, R0392) overnight at 293 K. The bacteria were harvested by centrifugation for 15 min at 5000 × g. Pellets were resuspended in 50 mM HEPES-NaOH (Roth, HN78, T135) pH 7.5, 200 mM NaCl (Th. Geyer, 1367), 5 mM 2-mercaptoethanol (β-ME) (SERVA 28,625), 1 mM phenylmethyl sulfonyl fluoride (PMSF) (Roth, 6367), 0.5% (v/v) Nonidet^{TM} P-40 substitute (Sigma-Aldrich, 74,385), and 0.3 mg/mL hen egg-white lysozyme (Applichem, A3711) and incubated on ice for 30 min. The cells were lysed by sonication and cellular debris was removed by centrifugation at 32,000 × g for 30 min. The supernatant was loaded onto either an amylose sepharose (NEB, E8201) or a glutathione Superflow agarose (Thermo Scientific, 25,237) column, depending on the respective purification tag, equilibrated with a buffer containing 50 mM HEPES pH 7.5, 300 mM NaCl, and 5 mM 2-mercaptoethanol. After washing with 10 column volumes of buffer the bound fusion protein was digested on column with tobacco etch virus (TEV) protease [25] overnight. The cleaved protein was eluted with column buffer, concentrated to a volume of 2 mL, and applied to a S200 16/600 size exclusion column (GE Healthcare) equilibrated with a buffer containing 20 mM HEPES-NaOH pH 7.5, 150 mM NaCl, and 2 mM DTT (Applichem, A2948). The peak fractions were pooled, concentrated and flash-frozen in liquid nitrogen. For preparation of seleno-methionine (SeMet) (Calbiochem, 561,505) substituted SidL and LegA11, proteins were expressed in *E. coli* BL21(DE3) following a protocol using PSM-5052 auto-induction medium [26].

Analytical size exclusion chromatography

Equimolar amounts of SidL and/or LegA11 in a total volume of 100 µL were applied to an S200 10/300 size exclusion column (GE Healthcare) equilibrated with buffer containing 20 mM HEPES pH 7.5, 150 mM NaCl, and 2 mM DTT at a flow rate of 0.5 ml/min. The concentrations used are given in the respective figure legends. The figures representing the chromatographic data were prepared using Origin (Version 2022b. OriginLab Corporation, Northampton, MA, USA).

Crystallization

Crystallization screening using various commercially available screens was performed in the 96-well format by mixing 200 nL of protein solution containing 12 mg/mL $SidL_{23–640}$, 5.2 mg/mL LegA11, and chymotrypsin, trypsin, or thermolysin (Sigma-Aldrich, C3142, T5266, P1512) in ratios between 1:500 to 1:2000 with 200 nL of reservoir solution in MRC plates using a Phoenix crystallization robot (Art Robbins Instruments, Sunnyvale, USA). The droplets were equilibrated against 50 µL reservoir solution at 291 K. Plate-shaped crystals grew in condition F1 (100 mM HEPES-NaOH pH 7.5 (Sigma-Aldrich, H3375, S7653), 200 mM L-proline (Sigma-Aldrich, 81,709), 100 g/L PEG3350 (Sigma-Aldrich, P4338)) of the Classics 2 screen (Qiagen, Hilden, Germany) in the presence of trypsin at 17 µg/mL. SeMet-derivatized crystals used for cryogenic data collection were grown in droplets of 1 µL protein (12 mg/mL $SidL_{23–640}$, 5.2 mg/mL LegA11, trypsin at 34 µg/mL) and 1 µL reservoir containing 100 mM HEPES-NaOH pH 7.5, 200 mM L-proline, and 200 g/L PEG3350 equilibrated against 200 µl reservoir solution. Crystals were cryoprotected by brief immersion in reservoir solution

containing 140 g/L PEG3350 and 23% (v/v) ethylene glycol (Sigma-Aldrich, 324,558) and flash-cooled in liquid nitrogen. Native crystals used for cryogenic data collection were grown in droplets of 1 µL protein (12 mg/mL $SidL_{23–640}$, 5.2 mg/mL LegA11, trypsin at 340 µg/mL) and 1 µL reservoir containing 100 mM HEPES-NaOH pH 7.5, 200 mM L-proline, and 140 g/L PEG3350 equilibrated against 200 µl reservoir solution. Crystals were cryoprotected by serial immersion in reservoir solutions containing 140 g/L PEG3350 and 0, 2, 4, 7, 10, 13, 16, 19, or 23% (v/v) glycerol (Sigma-Aldrich, 49,767) and flash-cooled in liquid nitrogen.

Data collection and processing

A dataset from a single native crystal was collected to a resolution of 2.35 Å at beamline PROXIMA 2A at the synchrotron SOLEIL (Gif-sur-Yvette Cedex, France) using a wavelength of 0.9762 Å. Four datasets were collected from a crystal grown from SeMet-substituted protein at a wavelength of 0.9795 Å at beamline P13 at the PETRA III storage ring (Hamburg, Germany) and merged to yield a complete highly redundant dataset to 3.3 Å. Data were processed with XDS and scaled with XSCALE [27,28]. For both crystals space group $P2_12_12_1$ could be assigned with unit cell dimensions of a = 68.5 Å, b = 93.4 Å, and c = 133.7 Å for the native crystal and of a = 657 Å, b = 974 Å, and c = 1307 Å for the SeMet-crystal, respectively

Structure solution and refinement

The structure was solved by the single anomalous dispersion (SAD) method employing the CRANK2 pipeline [29]. The initial electron density map was of sufficient quality for automatic building of 614 residues. The structure was iteratively completed and refined against the native data using Phenix.refine [30] followed by visual inspection and adjustment of the model in COOT [31] after each refinement cycle. Images showing structural data were prepared using Pymol (The PyMOL Molecular Graphics System, Version 1.8.6.2, Schrödinger, LLC). The data statistics are summarized in Table 1. The atomic coordinates and structure factors of SidL/LegA11 have been deposited in the Protein Data Bank (PDB entry 9SXC).

Isothermal titration calorimetry (ITC)

Binding between SidL (residues 76–645) and LegA11 (residues 1–269) was measured using a NanoITC 5302 microcalorimeter (Waters/TA Instruments) at 25°C. Proteins were prepared in 20 mM HEPES-NaOH (pH 7.5), 150 mM NaCl, degassed for 15 min at 30 mbar, and centrifuged at 20,000 × g for 5 min before titration. The sample cell (971 µL) contained SidL at 0.6 to 1.5 µM, with concentrations determined photometrically at 280 nm for each experiment. The syringe (100 µL) was loaded with 10 to 30 µM LegA11, also quantified by UV absorbance. Each experiment

Table 1. Data collection and refinement statistics.

	SidL/LegA11 native	SidL/LegA11 SeMet
Data collection		
Wavelength (Å)	0.978565	0.97950
Space group	P 21 21 21	P 21 21 21
Unit cell *a*, *b*, *c* (Å)	68.53, 93.38, 133.67	69.65, 97.38, 130.30
Resolution range (Å)	47.85 - 2.4 (2.486 - 2.4)[a]	78.003 – 3.3 (3.4 – 3.3)
$CC_{1/2}$[b]	0.999 (0.665)	0.999 (0.892)
R_{meas}[b]	0.1425 (1.411)	0.304 (2.02)
Total reflections	288,234 (37736)	696,282 (62675)
Unique reflections	41,606 (5384)	25,754 (2217)
Completeness (%)	99.70 (100.00)	100.00 (100.00)
Redundancy	6.9 (7.0)	27.0 (28.3)
$\langle I/\sigma(I)\rangle$	23.42 (2.04)	16.13 (3.87)
Structure refinement		
Resolution range (Å)	47.85 - 2.4 (2.47 – 2.40)	
R_{work}[c]	0.2244 (0.2995)	
R_{free}[d]	0.2672 (0.3812)	
No. of atoms	5658	
No. of protein atoms	5472	
No. of water molecules	186	
B-factors protein/water	66.71/59.32	
R.m.s.d. Bond lengths (Å)	0.003	
R.m.s.d. Bond angles (°)	0.56[ed]	
Protein Data Bank entry	###	

[a]The values in parentheses refer to statistics in the highest bin.
[b]$R_{meas} = \Sigma_{hkl}\,(n_{hkl}/n_{hkl} - 1)^{1/2}\,\Sigma_i|\langle I_{hkl}\rangle - I_{hkl,i}|/\Sigma_{hkl}\,\Sigma_i\,I_{hkl,i}$
[c]$R_{work} = \Sigma_{hkl}|F_o(hkl)\text{-}F_c(hkl)|/\Sigma_{hkl}F_o(hkl)$, where F_o and F_c are the observed and calculated structure-factor amplitudes, respectively.
[d]R_{free} was calculated with 5% of the data excluded from the refinement.
[e]R.m.s.d. = root mean square deviation.

consisted of 20 injections of 4.91 µL ligand, delivered at 200 rpm stirring speed with 400 s spacing. Buffer-into-protein control titrations were performed, and the resulting heats were subtracted from binding data. Thermograms were integrated using the NanoITC software, and binding isotherms were fitted in Origin (OriginLab) with an independent binding model. Parameters obtained directly from the fit included the stoichiometry (n), dissociation constant (K_d), and enthalpy change (ΔH); Gibbs free energy (ΔG), entropy (ΔS), and $-T\Delta S$ were calculated subsequently. Errors were estimated by error propagation, with asymmetric standard deviations reported for K_d. Data are representative of four independent experiments.

In vitro translation assay

Recombinant His_6-Myc-SidL and -LegA11 were expressed in *E. coli* BL21 (DE3) [14]. Overnight cultures were subcultured into LB (1%) and grown for 3 h at 37°C with shaking. Cultures were supplemented with 1 mM IPTG, grown overnight at 16°C, pelleted by centrifugation at 2100 × g for 10 min at 4°C, and washed in 5 mL of ice-cold PBS. Bacterial pellets were resuspended in ice-cold lysis buffer [His Binding buffer (Zymo His-Spin Protein Miniprep Kit),10 µg/mL lysozyme (Sigma, L6876), and 10 mM 2-mercaptoethanol (Sigma, M6250)] and incubated on ice for 2–4 h followed by sonication using Kontes Micro Ultrasonic Cell Disrupter (40 amplitude, 30 s, five times). Lysates were clarified via centrifugation at 9600 × g for 15 min at 4°C. Supernatants were transferred to clean microcentrifuge tubes and His-tagged proteins were then purified using the Zymo His-Spin Miniprep kit via manufacturer's instructions (Zymo Research). Purity was validated by SDS-PAGE and Coomassie Blue staining. Purified recombinant proteins were dialyzed overnight in PBS pH 7.4 at 4°C and quantified using the Coomassie Plus Bradford Assay (ThermoFisher, 23,238) reagent on a BioTek Epoch2 microplate reader (Agilent).

Translation of *Firefly* Luciferase mRNA in Rabbit Reticulocyte Lysates was quantified using the Flexi Rabbit Reticulocyte Kit (Promega, Madison, WI) [14]. Purified recombinant His_6-Myc-SidL (50 ng) and/or His_6-Myc-LegA11 (23.3 ng) were added to lysates in equimolar amounts (65 nM). Reactions were run in triplicate for 90 min at 30°C followed by addition of Luciferase assay reagent (Promega, E1483) and luminescence (arbitrary units) was quantified using a BioTek Synergy HTX multimode plate reader (Agilent).

L. pneumophila growth curves

L. pneumophila was cultured on CYE agar at 37°C and single colonies were used to generate 2-day heavy patches. One day prior to infection, *A. castellanii* cultures were split 1:5 into 75 cm^2 tissue culture flasks and incubated in PYG media at 25°C. Cells were seeded in 24-well tissue culture-treated dishes (2.5 $\times 10^5$ cells/well) in 1 mL PYG and incubated at 37°C for 2 h. Adhered cells were washed in pre-warmed Ac buffer (0.4 mM $CaCl_2$, 4 mM $MgSO_4$, 3.4 mM Na citrate, 0.05 mM $F_3(NH_4)_2(SO_4)_2$, 2.5 mM Na_2HPO_4, 2.5 mM KH_2PO_4, pH 6.5) and infected with heavy-patch grown *L. pneumophila* [multiplicity of infection (MOI) of 0.1] in 1 mL Ac buffer in triplicate wells. Cells were incubated for 45 min and monolayers were washed three times with PBS to remove extracellular bacteria. Cells were either lysed (bacterial uptake) or incubated in 1 mL Ac buffer for up to 72 h at 37°C. Cells were lysed hypotonically in sterile deionized water and lysates were plated on CYE agar for enumeration of colony forming units (CFU) at 45 min, 24 h, 48 h, and 72 h post-infection [18].

To quantify *L. pneumophila* growth *in vitro*, 2-day heavy patches grown on CYE agar were resuspended in supplemented AYE broth and subcultured to an OD_{600} of 0.2. Cultures were dispensed into sterile 96-well round bottom plates ($n = 6$/strain) and incubated with continuous orbital shaking in a BioTek Epoch2 microplate reader. Data were collected every 2 h for up to 46 h.

Statistical analyses

Data are shown as mean ± standard deviation (s.d.) or standard error (s.e.m), as indicated. Statistical analyses were performed with GraphPad Prism 10 using either Welch's t-test, one-way ANOVA, or two-way ANOVA, as described, with statistical significance defined as $p < 0.05$. Unless otherwise indicated, statistical analyses were performed on biological triplicate samples ($N = 3$) and representative of three independent experiments.

Results

SidL directly interacts with LegA11 forming a stable 1:1 complex

LegA11 was initially identified as a metaeffector based on its ability to suppress the toxic effect of SidL in a heterologous yeast expression system and bind to SidL in yeast two-hybrid and LUMIER assays [16].

A direct protein-protein interaction between purified recombinant SidL and LegA11 was recently validated [11], but the kinetics and biophysical properties of the SidL-LegA11 interaction are unknown. To verify the direct interaction of SidL and LegA11 and assess the stoichiometry of the SidL-LegA11 complex, we subjected purified recombinant full-length $SidL_{1–666}$, LegA11, or equimolar amounts of $SidL_{1–666}$ and LegA11 to analytical size exclusion chromatography (SEC). In the chromatogram corresponding to the mixture, the peaks of the single proteins have merged into a single peak shifted to a lower elution volume (Figure 1). This indicates that SidL and LegA11 form a stable complex with 1:1 stoichiometry.

We employed X-ray crystallography to visualize the SidL/LegA11 complex. Full-length SidL could not be purified in amounts large enough for an extended crystallization campaign; thus, we used the truncated variant $SidL_{23–640}$ for overexpression as it could be produced in higher yield and displayed higher stability than the full-length protein. We set up crystallization trials using various commercial screens with an equimolar mixture of SidL and LegA11 but did not obtain any crystals. We then used *in situ* proteolysis [32] by adding various proteases to the crystallization setups (see *Materials and Methods*). We obtained crystals in several conditions, the best of which diffracted X-rays to a resolution limit of 2.4 Å after optimization. We solved the structure by SAD using data from a crystal composed of selenomethionine-substituted protein. Crystallographic details are given in Table 1.

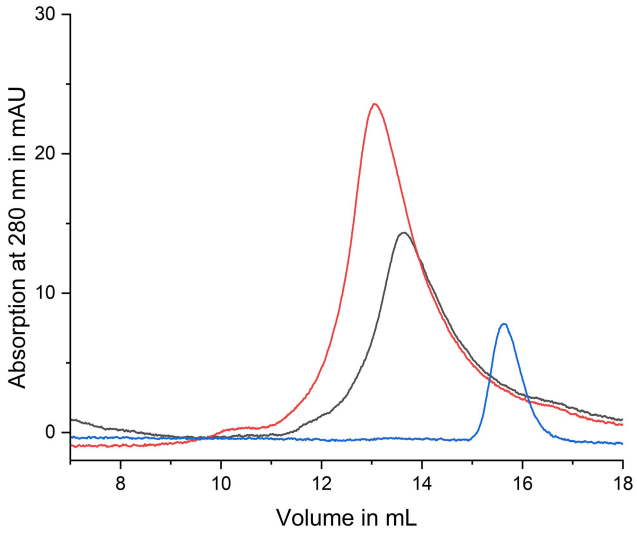

Figure 1. Interaction of SidL and LegA11 observed in analytical size exclusion chromatography. 300 µg $SidL_{1–666}$ and/or 125 µg LegA11 in 100 µL buffer were applied to an S200 10/300 increase size exclusion column. The absorption curve of $SidL_{1–666}$ is shown in black, the absorption curve of LegA11 is shown in blue, the absorption curve of the mixed proteins is shown in red.

The crystal structure contains residues 76–313, 334–413, and 525–628 of SidL and residues 7–192, and 202–261 of LegA11, as well as 186 water molecules. SidL is divided into two subdomains comprising residues 76–222 ($SidL_N$) and residues 228–628 ($SidL_C$), respectively (Figure 2). $SidL_N$ is connected to $SidL_C$ via a straight elongated stretch of five residues (223–227). The two subdomains are separated by a C-terminal portion of LegA11 and do not interact with each other directly. Presumably, in the absence of LegA11 the domains display a high degree of conformational flexibility.

$SidL_N$ consists of eight rather short helices (α1-α8) that form pairs, which are aligned in a nearly parallel fashion except for the second pair, where α4 is tilted by about 50° (Figure 2). The order of the helix pairs is α3/α4, α1/α2, α5/α6, and α7/α8. Helices within pairs are connected via short loops, whereas the pairs are interconnected by longer loops. $SidL_C$ displays an elongated shape that is roughly divided into two parts. The first part contains helices α9-α13 that are arranged in parallel layers of three (α9-α11) and two (α12 and α13). The helix axes are oriented roughly parallel to each other. This part is completed by the C-terminal helix α23 that packs against the three-helix layer in an orthogonal fashion. The second part is composed of the helix pair α16 and α17 that packs orthogonally against a helix bundle formed by helices α18-α21. Both parts are connected via helix α14 that interacts with α23 and α19 and the short helix α22 preceding the terminal helix α23. α14 and α16 are connected via a long loop of 20 residues that contain the single-turn helix α15. Between α17 and α18, about 110 residues are missing that presumably have been removed by the protease used for crystallization.

The N-terminal part of LegA11 is formed by four ankyrin repeats, of which the first three display the typical arrangement of short, paired helices (α1'/α2,' α3'/α4,' α5'/α6') with the connecting loops between pairs protruding at an angle of approximately 90° [33]. The fourth repeat (α7'/α8') deviates from the other three through longer helices and a shortened loop between the third and fourth repeat. The first three repeats correspond to a previously published crystal structure (PDB ID 4ZHB) comprising residues 11–114. Both structures can be superimposed with a root mean square deviation of 0.52 Å. The fourth repeat is immediately followed by a pair of very short helices, α9' and α10.' These helices are oriented roughly perpendicular to each other and are connected via a twisted two-stranded anti-parallel β-sheet formed by strands β1' and β2.' The β-sheet is "wrapped" by the

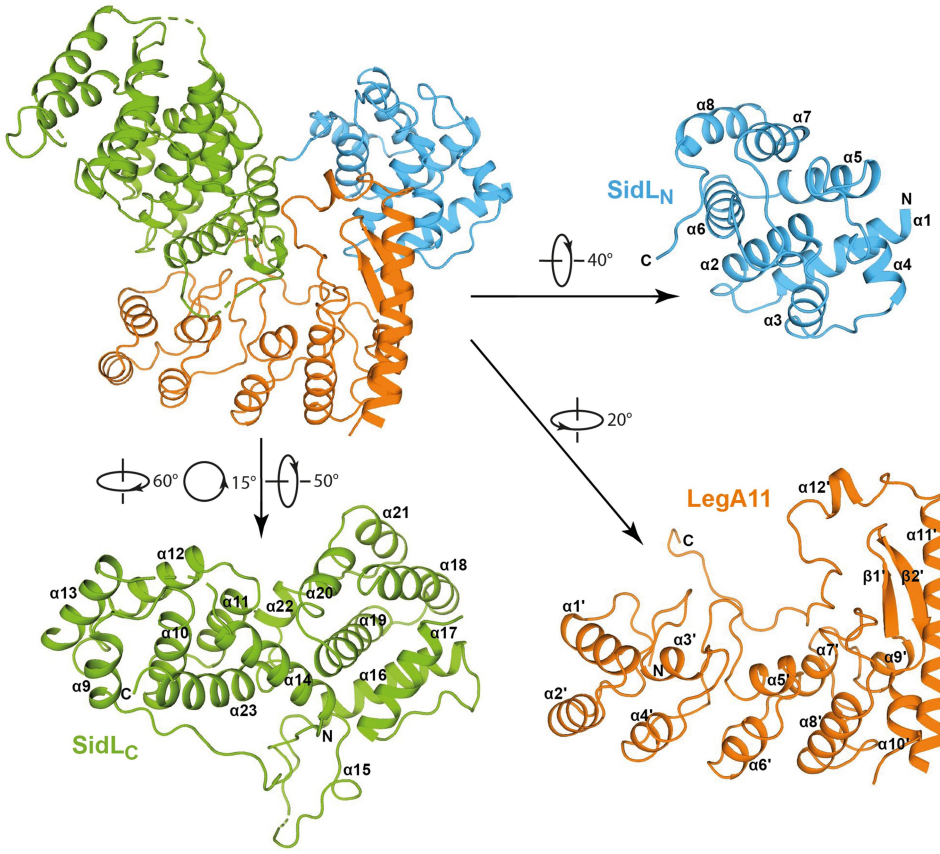

Figure 2. Overall structure of SidL/LegA11. Cartoon representation of the three-dimensional structure of the complex formed by SidL and LegA11. The model in the upper left corner represents the complex. The two subdomains of SidL are shown in blue and green, LegA11 is shown in orange. For better visibility, the complex components have been rotated individually, the respective degrees of rotation relative to the orientation of the complex are shown next to the arrows. Secondary structure elements as well as the n- and C-termini of the individual components are labeled.

long helix α11' following helix α10' on one side, the single-turn helix α12' at the top, and an extended loop on the other side. The overall shape resembles the letter L with the ankyrin repeats forming the stalk and the C-terminal extension forming the base.

A search for structural homologs using the DALI server with SidL$_N$ as search model did not yield significantly similar structures. An equivalent search using SidL$_C$ as search model identified the recently published cryo-EM structure of the *Legionella* effector LnaB (PDB ID 8JO4) as the closest structural homolog. Superposition of SidL$_C$ with the N-terminal domain of LnaB yielded an r.m.s.d. value of 2.7 Å for 201 equivalent Cα atoms (Suppl. Fig. S1). The identity of the aligned sequence stretches is 21.9%.

Characterization of the SidL/LegA11 binding interface

SidL interacts with LegA11 via an interface of about 2300 Å^2 as determined by PISA and sppIDER [34,35]. SidL$_C$ contacts LegA11 via the inside of both the stalk and the base of the L-shape with an interaction surface of about 1500 Å^2, whereas SidL$_N$ is placed on the opposite side of the base of LegA11 (Figure 2). The interaction of SidL$_N$ and LegA11 is mediated via several polar side chain-main chain interactions, for instance between the side chain of K180 of LegA11 with the main chain oxygen of R121 of SidL or the side chain of E118 of SidL with the main chain nitrogen of I178 of LegA11, respectively (Figure 3(A)). The only charged side chain-side chain interaction is between K224 of LegA11 and E118 of SidL$_N$. Hydrophobic interactions involve residues L99 and L103 in SidL$_N$ and L232, I236, F239, and F240 in LegA11. The interaction between SidL$_C$ and LegA11 is mainly mediated by polar and charged interactions, whereas distinct hydrophobic interactions are absent (Figure 3(B)). In the following description, the respective residue of SidL$_C$ will be mentioned first. Salt bridges are formed between the side chains of D393 and of K86 and the side chains of R396 and of E254, respectively. Side chain-main chain interactions are visible between the

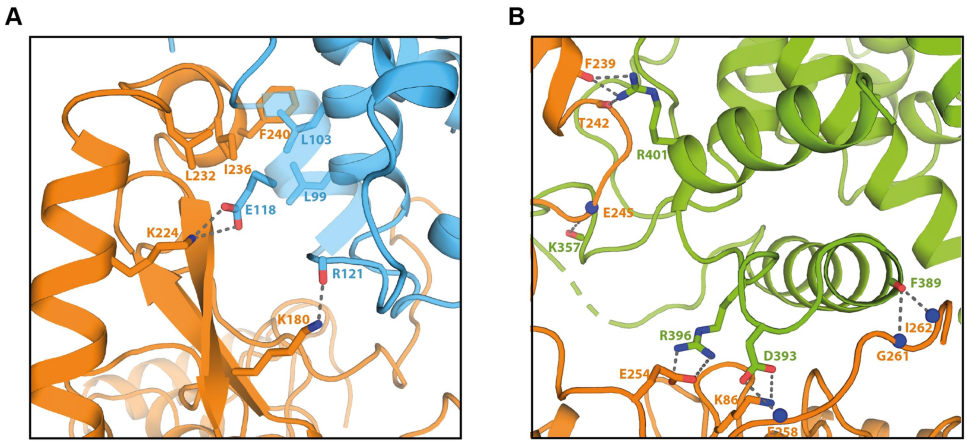

Figure 3. Binding interfaces of SidL and LegA11. Cartoon representation of the binding interfaces between SidL and LegA11. The color code corresponds to that in Figure 2. Side chains of amino acid residues responsible for mediating the interactions are depicted as stick models and are labeled accordingly. Hydrogen bonds and polar interaction are shown as gray dotted lines. (a) interface between $SidL_N$ and LegA11. (b) interface between $SidL_C$ and LegA11.

side chain of D393 and the main chain nitrogen of E258, as well as of R401 and the carbonyl oxygens of F239 and T242. Main chain-main chain interactions exist between the carbonyl oxygen of K357 and the nitrogen of E245, and the carbonyl oxygen of F389 and the nitrogens of G261 and I262.

To determine the binding affinity of SidL and LegA11, we employed isothermal titration calorimetry (ITC) using purified proteins. Based on the domain boundaries of SidL seen in the crystal structure, we recombinantly produced the variant $SidL_{76–628}$, but found the protein to be contaminated with a degradation product. Extending the C-terminus to residue K645 yielded a stable protein that could be purified with high purity and yield, which was used in subsequent ITC experiments. We performed ITC measurements with SidL in the sample cell at concentrations between 1.45 and 0.61 µM and a 20-fold molar excess of LegA11 in the syringe. Averaging the individual measurements, we obtained a dissociation constant of 1.8 nM (Figure 4).

To verify the binding interface between SidL and LegA11 seen in the crystal structure, we introduced

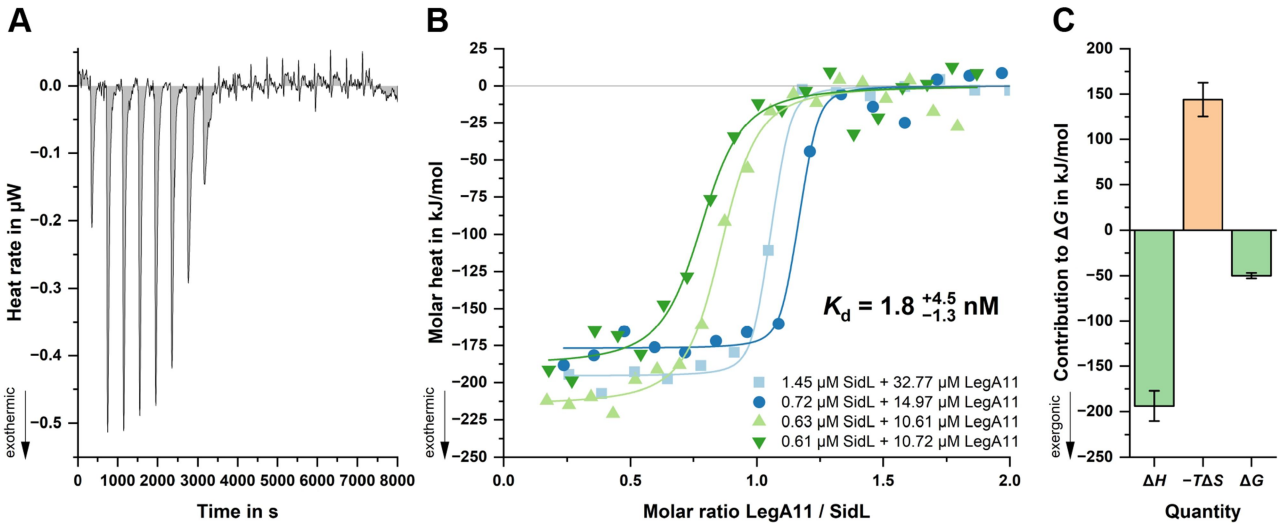

Figure 4. Affinity of SidL and LegA11 determined by ITC. (a) baseline-corrected heat rate (µW) versus time (s) for titration of LegA11 (ligand) into SidL (receptor) at 25 °C, showing exothermic binding events (negative peaks) that diminish after saturation. (b) integrated binding isotherms from four independent experiments plotted as molar heat (kJ/mol) versus molar ratio of LegA11 to SidL. The best-fit one-site model yielded a dissociation constant K_d of 1.8 $^{+4.5}_{-1.3}$ nM, with a stoichiometry of 0.92 ± 0.16. Binding was strongly exothermic (average $\Delta H \approx -200$ kJ/mol). Receptor and ligand concentrations were: 1.45/32.77 µM, 0.72/14.97 µM, 0.63/10.61 µM, and 0.61/10.72 µM (SidL/lega11). C. Thermodynamic signature of binding showing large enthalpic contribution ($\Delta H = -194 \pm 17$ kJ/mol) opposed by an unfavorable entropic term ($-T\Delta S = +144 \pm 16$ kJ/mol), resulting in a free energy change of $\Delta G = -50 \pm 3$ kJ/mol.

mutations into LegA11 to disturb complex formation. Given the large size of the interface, we decided to pursue a rather drastic approach by generating the quadruple mutant K95A/F239R/F240R/G243R. The three latter residues are located near the subdomain linker of SidL. We reasoned that introducing three charged long-chain residues into this tight hydrophobic pocket would increase the chances of disrupting the binding interaction between SidL and LegA11. We purified the resulting protein (LegA11-4 M) to homogeneity, and subjected $SidL_{76–645}$ alone, LegA11 in wild-type or mutant form alone, or in equimolar ratio with $SidL_{76–645}$ to analytical size exclusion chromatography (SEC). As expected, wild-type LegA11 formed a stable complex with the truncated SidL variant (Figure 5). The chromatogram corresponding to $SidL_{76–645}$ and LegA11-4 M shows two distinct peaks very close to the positions of the single proteins. The slight shift to lower elution volumes most likely reflects a very weak transient interaction between $SidL_{76–645}$ and LegA11-4 M. These data suggest that the interface observed in the crystal structure is indeed responsible for binding of LegA11 to SidL and that the interaction is largely abrogated by introduction of the mutations.

LegA11 restores SidL-inhibited mRNA translation via a direct protein-protein interaction

Of the eight *L. pneumophila* effectors that block eukaryotic mRNA translation, two are associated with metaeffectors. The translation inhibiting effects of SidI are completely abolished in the presence of its metaeffector, MesI [14]. Therefore, we evaluated the effects of LegA11 on SidL-mediated translation inhibition. Recombinant His_6-Myc-SidL and -LegA11 were purified from *E. coli* (Suppl. Fig S2) and added to cell-free rabbit reticulocyte lysates to quantify luciferase (Luc) mRNA translation. SidL inhibited Luc mRNA translation in a dose-dependent manner but with less potency than the effector SidI (Figure 6(A)), validating results from a prior study [9]. LegA11 binds and abrogates SidL toxicity in a heterologous yeast expression system [16]; thus, we tested the hypothesis that LegA11 suppresses SidL-mediated translation inhibition. Translation increased significantly when equimolar amounts of LegA11 and SidL were added to reactions and did not differ from reactions containing LegA11 alone (Figure 6(B)). Thus, LegA11 binds and suppresses SidL activity, further validating its role as a metaeffector of SidL.

We hypothesized that SidL-LegA11 complex formation is required for functional regulation of SidL. To test this, we quantified Luc mRNA translation in cell-free lysates containing equimolar amounts of purified recombinant SidL with either wild-type LegA11 or LegA11-4 M (Suppl. Fig. S2), the latter of which has lost the ability to bind SidL (Figure 5). SidL-mediated translation inhibition was suppressed by wild-type LegA11 but unaffected by LegA11-4 M since the extent of translation inhibition did not differ from reactions containing SidL alone (Figure 6(C)). Luc mRNA translation was not affected by either wild-type LegA11 or LegA11-4 M alone (Figure 6(C)). Together, these data show that LegA11 regulates SidL via a direct protein-protein interaction and that SidL is unable to inhibit translation when it is bound to LegA11.

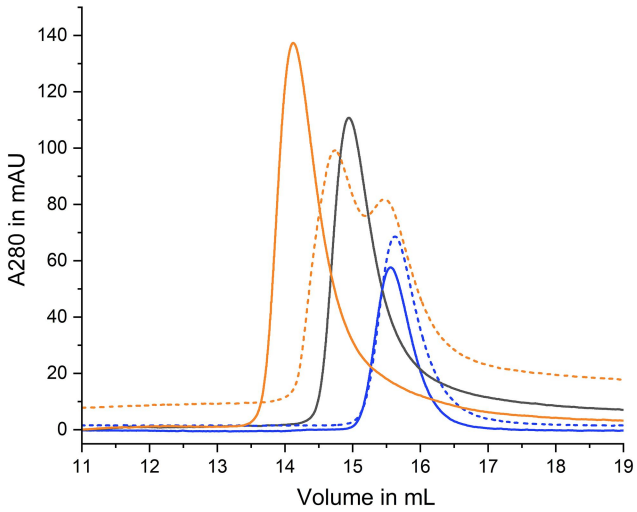

Figure 5. Influence of mutations in LegA11 on binding to $SidL_{76–645}$. 1 mg $SidL_{76–645}$ and/or 400 µg LegA11 in 100 µL buffer were applied to an S200 10/300 increase size exclusion column. The colors of the respective chromatograms are as follows: $SidL_{76–645}$ – black; LegA11-WT – blue; LegA11-4 M – dotted blue; $SidL_{76–645}$/LegA11-WT – orange; $SidL_{76–645}$/LegA11-4 M – dotted orange.

Neither SidL nor LegA11 impact L. pneumophila replication

He *et al.* found that neither SidL nor LegA11 individually influence *L. pneumophila* replication within primary bone marrow-derived macrophages (BMDMs) from susceptible A/J mice and the social amoebae, *Dictyostelium discoideum* [11]. *D. discoideum* is routinely used as a model to study *L. pneumophila* in the laboratory [36,37]; however, a single protozoan host is unable to capture the diversity of hosts and niches experienced by *L. pneumophila* in the environment [38,39]. To determine whether SidL or LegA11 influence *L. pneumophila* replication within a natural protozoan host, *L. pneumophila* strains with clean unmarked chromosomal deletions of *legA11* or *sidL* (Δ*legA11* or Δ*sidL*, respectively) were generated to assess replication within *Acanthamoeba castellanii*. We found no differences in *L. pneumophila* Δ*legA11* or Δ*sidL* growth relative to

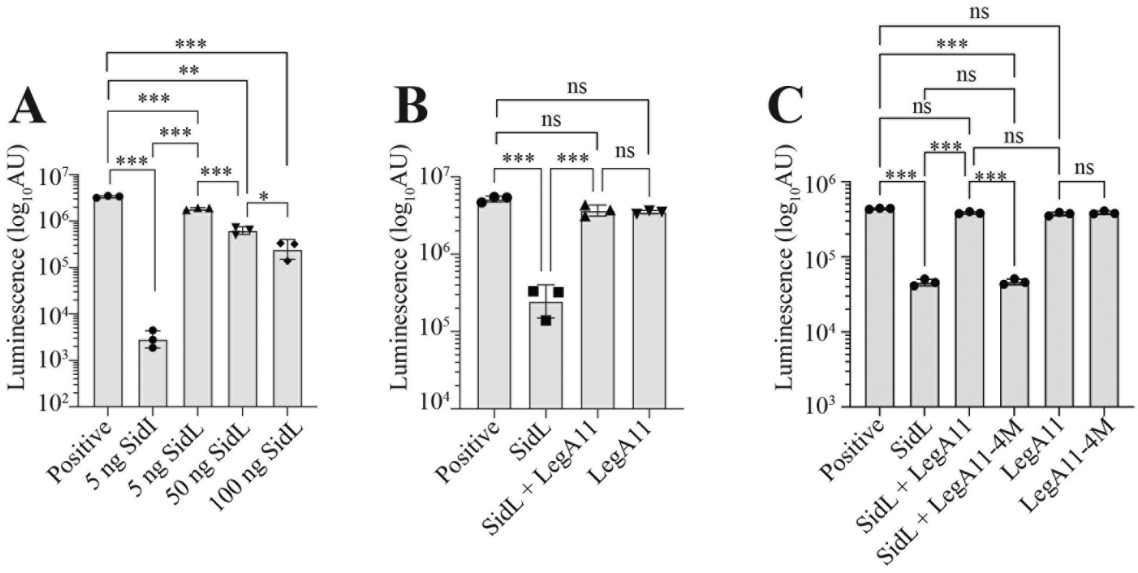

Figure 6. LegA11 restores SidL-mediated translation inhibition via a direct protein-protein interaction. Rabbit reticulocyte lysates were incubated with firefly luciferase (Luc) mRNA alone (positive) or with **(a)** 5 ng SidI, 5ng SidL, 50 ng SidL, or 100 ng SidL; **(b)** 65 nM of SidL, SidL and LegA11, or LegA11 alone; or **(c)** 65 nM of SidL alone, SidL and LegA11 variants, or LegA11 variants alone. Data shown are mean ± standard deviation (s.d.) of samples in triplicates ($N = 3$) and are representative of three independent experiments. AU, arbitrary units. Asterisks (*) denote statistical significance (***$p < 0.001$, *$p < 0.05$, ns, not significant) by one-way ANOVA with Tukey's post-hoc test.

either wild-type *L. pneumophila* or genetically complemented strains in *A. castellanii* (Suppl. Fig S3A). We also found no differences in growth in AYE broth *in vitro* (Suppl. Fig. S3B). These findings support prior data suggesting that SidL and LegA11, like many *L. pneumophila* effectors, may function redundantly with other effectors in *A. castellanii* and/or have a more pronounced role in other *L. pneumophila* host(s) [38,39].

Discussion

Over the past decade, a growing number of metaeffectors have been identified and functionally characterized [12,14–16,18,40]. Metaeffectors are effectors that regulate cognate effector(s) by direct physical interactions [13], which is distinct from effector pairs that act in an opposing manner on the same host proteins and processes [41–43]. LegA11 was recently validated as a metaeffector of SidL [11,16], but the role of the SidL-LegA11 interaction in LegA11's metaeffector activity was not fully established. Using purified proteins, we found that SidL and LegA11 bind with high affinity to form a stable binary complex, which prompted us to attempt a crystallographic characterization of the complex. Despite extensive crystallization trials using different N- and C-terminal truncation variants of SidL, we only obtained crystals after adding trace amounts of protease. This suggests that SidL contains one or more flexible regions that counteract crystal formation and is in line with the observation that SidL in the crystal structure is further truncated both N- and C-terminally than our shortest construct used for crystallization. Furthermore, a portion of 110 amino acid residues (aa 414–524) had been removed from $SidL_C$ opposite the LegA11 binding site, which may indicate that this portion is flexible in the absence of a putative second binding partner.

SidL and LegA11 interact via a rather large interface of about 2300 $Å^2$ involving mostly charged or polar side chains (Figure 2 and 3). Although such an interface size suggests biological relevance [44], we wanted to verify that this interface is not a crystallization artifact. Indeed, mutagenesis of four interface residues in LegA11 (LegA11-4 M) disrupted the interaction between the two proteins. We found that LegA11-4 M was unable to form a complex with SidL (Figure 5), confirming the validity of the interface seen in the crystal structure (Figure 3(A,B)). The inability of LegA11-4 M to functionally regulate SidL *in vitro* (Figure 6(C)) suggests that LegA11's metaeffector activity is mediated by a direct protein-protein interaction with SidL. A very recent study included a model of the complex between SidL and LegA11 generated with AlphaFold2 (He et al. 2025). The authors of this study described fourteen polar interactions between LegA11 and SidL. We compared these interactions to those found in our crystal structure. We could confirm the

interactions of R17 and K180 from LegA11 with D549 and R121 from SidL, respectively. I2 and R6 are not resolved in our structure, which indicates that these residues do not form stable interactions within the complex. The remaining ten side chains of LegA11 are in the vicinity of their respective postulated interaction partners in SidL, but they are either not in hydrogen bonding distance or in a relative geometry that precludes hydrogen bond formation. This comparison suggests that AlphaFold2 correctly identified the interaction interface, but that details of the interaction on the level of single residues require experimental structural data.

SidL is one of at least eight *Legionella* effectors able to inhibit host mRNA translation *in vitro* [45–47]. The translation-inhibiting effector SidI (Lpg2504) is also regulated by a metaeffector, MesI (Metaeffector of SidI; Lpg2505). Like SidL and LegA11, SidI and MesI also form a high-affinity 1:1 complex that renders SidI nontoxic and unable to suppress mRNA translation [14]. Moreover, LegA11 and MesI both bind their cognate effectors – SidL and SidI, respectively – within *L. pneumophila*. The stability of these effector-metaeffector binary complexes may explain why less SidL and SidI are translocated into host cells when their cognate metaeffectors are present [11,48]. We found that LegA11's metaeffector activity is mediated by a direct protein-protein interaction with SidL, but whether the same binding interface is responsible formation SidL-LegA11 regulation within living cells remains to be elucidated. We are currently testing whether LegA11-4 M can bind SidL within *L. pneumophila* and/or regulate SidL translocation into host cells.

A very recent study describes SidL as an ATPase that hydrolyzes ATP to AMP and pyrophosphate [11]. SidL binds ATP via an S-HxxxE motif [11], which is also present in toxins from phylogenetically diverse bacterial species [49]. He et al. [11] suggested that the inhibitory effect of LegA11 is exerted via binding to the C-terminal domain of SidL, where the active center is located [11]. To examine the spatial relationship between LegA11 and the ATP-binding site, we generated an AlphaFold3 (AF3) model of SidL complexed with ATP and superposed it with the SidL from our crystal structure. From the superposition it is apparent that LegA11 does not bind in the vicinity of the active site (Suppl. Fig. S4). Thus, it is unlikely that LegA11 abolishes ATP hydrolysis by directly occluding the nucleotide binding site of SidL. A structure of the effector RavJ in complex with its metaeffector LegL1 revealed that allosteric regulation is not a universal feature of metaeffectors LegL1 binds and occludes the active site of RavJ [16]. Thus, metaeffector regulatory mechanisms are diverse and can be defined experimentally through structural studies.

Despite functional similarities, SidL and SidI are mechanistically distinct. SidI is a mannosyltransferase that directly inactivates the host mRNA translation machinery [9,14]. Moreover, unlike SidL, the enzymatic activity of SidI is independent of host co-factors and requires only its activated sugar donor, GDP-mannose, for catalysis [14]. While SidI can function within *L. pneumophila* by itself [50], the requirement for host actin as a co-factor provides a plausible explanation for lack of discernable intrabacterial SidL activity (Suppl. Fig S3B). The mechanism of SidL-mediated translation inhibition has not been defined. He et al. suggest that SidL functions to deplete host cytosolic ATP pools [11], which could plausibly limit mRNA translation; however, it is also tempting to speculate a mechanistic connection between impaired actin polymerization and translation since F-actin serves as a scaffold for polyribosome assembly [9,51–55]. Sustained translation on monoribosomes may explain why SidL blocks translation with less potency than SidI (Figure 6A) [9].

SidL's requirement for globular actin as an activating co-factor is similar to actin-mediated activation of the *Legionella* effector LnaB [11,49,56]. He *et al.* found that SidL binds LegA11 and actin simultaneously [11], which we corroborated using AF3 to generate a hypothetical ternary complex by overlaying SidL from our crystal structure with the SidL from the actin complex (Suppl Figure 5). Indeed, the binding sites of LegA11 and actin do not overlap, confirming the experimental findings of He et al. [11]. Interestingly, in all 15 AF3 predictions, $SidL_C$ is sufficient for binding actin, whereas $SidL_N$ is able to assume a wide variety of conformations (Suppl. Fig. S6). This is in line with the binding mode of actin in several crystal structures with LnaB, which does not possess a subdomain corresponding to $SidL_N$. It is evident from our crystal structure that upon binding, LegA11 abolishes the conformational flexibility of $SidL_N$ and locks it in a fixed orientation relative to $SidL_C$. This conformational restriction is also likely reflected in the unusually high loss of entropy ($-T\Delta S = 144$ kJ/mol) seen in our ITC measurements (Figure 4).

A recent structural study showed that actin enhances the affinity of LnaB for its target phosphoribosyl-ubiquitin (PR-Ub) [57]. According to these authors' model, the hydrolysis incompetent binary complex formed by LnaB and actin is activated by binding of PR-Ub. However, for SidL no third protein is required, since purified SidL and actin are sufficient for efficient ATP hydrolysis [11]. Therefore, actin must play a direct role in inducing hydrolytic competence. The most

likely scenario is that binding of actin orders the large flexible loop (aa 414–524) of SidL, which at its C-terminal end borders on the nucleotide binding site. This reorientation may position loop residues required for nucleotide hydrolysis in a catalytically competent fashion. We hypothesize that the fixed N-terminal domain seen in our crystal structure prevents the correct positioning of the loop, effectively rendering SidL catalytically inactive despite concomitant binding of actin. However, elucidation of the precise mechanisms of both activation by actin and inhibition by LegA11 will require structural characterization of the respective complexes in the future.

Acknowledgements

We thank Petra Hinse for excellent technical assistance, Dr. Craig Roy (Yale University) for providing pSN85 and pSR47S plasmids, and Dr. Brian Geisbrecht (Kansas State University) for helpful discussions and providing the pT7HMT plasmid.

Author contributions

CRediT: **Dominik A. Machtens:** Data curation, Formal analysis, Investigation, Methodology, Validation, Writing – review & editing; **Carissa A. Hutchison:** Data curation, Formal analysis, Investigation, Methodology, Validation, Visualization, Writing – review & editing; **Ashley M. Stein:** Data curation, Formal analysis, Investigation, Methodology, Validation, Writing – original draft, Writing – review & editing; **Jan Eberhage:** Data curation, Formal analysis, Investigation, Methodology, Validation, Visualization, Writing – review & editing; **Jonas M. Willerding:** Data curation, Formal analysis, Investigation, Methodology, Validation, Writing – review & editing; **Susanne Eschenburg:** Data curation, Investigation, Methodology, Supervision, Writing – review & editing; **Stephanie R. Shames:** Conceptualization, Data curation, Formal analysis, Funding acquisition, Methodology, Project administration, Supervision, Validation, Visualization, Writing – original draft, Writing – review & editing; **Thomas F. Reubold:** Conceptualization, Data curation, Formal analysis, Investigation, Methodology, Project administration, Supervision, Validation, Visualization, Writing – original draft, Writing – review & editing.

Funding

Work in the Shames lab was supported by the National Institutes of Health [P20GM113117] and start-up funds from Kansas State University and Michigan State University.

Disclosure statement

No potential conflict of interest was reported by the author(s).

Data availability statement

The authors confirm that the data supporting the findings of this study are available within the article and doi:10.6084/m9.figshare.30428647.

ORCID

Dominik A. Machtens http://orcid.org/0000-0002-1597-7901
Carissa A. Hutchison http://orcid.org/0000-0002-2560-931X
Ashley M. Stein http://orcid.org/0000-0001-9098-7563
Jan Eberhage http://orcid.org/0000-0002-6101-9667
Jonas M. Willerding http://orcid.org/0000-0001-8281-5024
Susanne Eschenburg http://orcid.org/0000-0002-7422-618X
Stephanie R. Shames http://orcid.org/0000-0002-2278-1405
Thomas F. Reubold http://orcid.org/0000-0001-8034-5313

References

[1] Gomez-Valero L, Buchrieser C. Intracellular parasitism, the driving force of evolution of Legionella pneumophila and the genus *Legionella*. Microbes Infect. 2019;21(5–6):230–236. doi: 10.1016/j.micinf.2019.06.012
[2] Lockwood DC, Amin H, Costa TRD, et al. The *Legionella pneumophila* Dot/Icm type IV secretion system and its effectors. Microbiol (Read). 2022;168(5):168. doi: 10.1099/mic.0.001187
[3] Mondino S, Schmidt S, Rolando M, et al. Legionnaires' disease: state of the art knowledge of pathogenesis mechanisms of *Legionella*. Annu Rev Pathol. 2020;15(1):439–466. doi: 10.1146/annurev-pathmechdis-012419-032742
[4] Romanov KA, O'Connor TJ. *Legionella pneumophila*, a Rosetta stone to understanding bacterial pathogenesis. J Bacteriol. 2024;206(12):e0032424. doi: 10.1128/jb.00324-24
[5] Belyi Y, Tabakova I, Stahl M, et al. Lgt: a family of cytotoxic glucosyltransferases produced by *Legionella pneumophila*. J Bacteriol. 2008;190(8):3026–3035. doi: 10.1128/JB.01798-07
[6] Belyi Y, Jank T, Aktories K. Effector glycosyltransferases in *Legionella*. Front Microbiol. 2011;2:76. doi: 10.3389/fmicb.2011.00076
[7] Moss SM, Taylor IR, Ruggero D, et al. A *Legionella pneumophila* kinase phosphorylates the Hsp70 chaperone family to inhibit eukaryotic protein synthesis. Cell Host Microbe. 2019;25:454–462.e6. doi: 10.1016/j.chom.2019.01.006
[8] Syriste L, Patel DT, Stogios PJ, et al. An acetyltransferase effector conserved across *Legionella* species targets the eukaryotic eIF3 complex to modulate protein translation. MBio. 2024;15(3):e0322123. doi: 10.1128/mbio.03221-23
[9] Subramanian A, Wang L, Moss T, et al. A *Legionella* toxin exhibits tRNA mimicry and glycosyl transferase activity to target the translation machinery and trigger

a ribotoxic stress response. Nat Cell Biol. 2023;25 (11):1600–1615. doi: 10.1038/s41556-023-01248-z
[10] Guo Z, Stephenson R, Qiu J, et al. A *Legionella* effector modulates host cytoskeletal structure by inhibiting actin polymerization. Microbes Infect. 2014;16 (3):225–236. doi: 10.1016/j.micinf.2013.11.007
[11] He C, Li C, Liu Y, et al. Modulation of host ATP levels by secreted bacterial effectors. Nat Commun. 2025;16 (1):4675. doi: 10.1038/s41467-025-60046-3
[12] Kubori T, Shinzawa N, Kanuka H, et al. *Legionella* metaeffector exploits host proteasome to temporally regulate cognate effector. PLOS Pathog. 2010;6(12): e1001216. doi: 10.1371/journal.ppat.1001216
[13] Joseph AM, Shames SR. Affecting the effectors: regulation of *Legionella pneumophila* effector function by metaeffectors. Pathogens. 2021;10(2):108. doi: 10.3390/pathogens10020108
[14] Joseph AM, Pohl AE, Ball TJ, et al. The *Legionella pneumophila* metaeffector Lpg2505 (MesI) regulates SidI-mediated translation inhibition and novel glycosyl hydrolase activity. Infect Immun. 2020;88(5). doi: 10.1128/IAI.00853-19
[15] Machtens DA, Willerding JM, Eschenburg S, et al. Crystal structure of the metaeffector MesI (Lpg2505) from *Legionella pneumophila*. Biochem Biophys Res Commun. 2020;527:696–701. doi: 10.1016/j.bbrc.2020.05.027
[16] Urbanus ML, Quaile AT, Stogios PJ, et al. Diverse mechanisms of metaeffector activity in an intracellular bacterial pathogen, *Legionella pneumophila*. Mol Syst Biol. 2016;12(12):893. doi: 10.15252/msb.20167381
[17] Machtens DA, Hutchison CA, Stein AM, et al. Crystal structure of the *Legionella pneumophila* effector SidL (Lpg0437) in complex with its metaeffector LegA11 (Lpg0436). BioRxiv. 2025. doi: 10.1101/2025.10.23.683979
[18] Shames SR, Liu L, Havey JC, et al. Multiple *Legionella pneumophila* effector virulence phenotypes revealed through high-throughput analysis of targeted mutant libraries. Proc Natl Acad Sci USA. 2017;114(48): E10446–E10454. doi: 10.1073/pnas.1708553114
[19] Feeley JC, Gibson RJ, Gorman GW, et al. Charcoal-yeast extract agar: primary isolation medium for *Legionella pneumophila*. J Clin Microbiol. 1979;10 (4):437–441. doi: 10.1128/jcm.10.4.437-441.1979
[20] Moffat JF, Tompkins LS. A quantitative model of intracellular growth of *Legionella pneumophila* in *Acanthamoeba castellanii*. Infect Immun. 1992;60 (1):296–301. doi: 10.1128/iai.60.1.296-301.1992
[21] Geisbrecht BV, Bouyain S, Pop M. An optimized system for expression and purification of secreted bacterial proteins. Protein Expr Purif. 2006;46(1):23–32. doi: 10.1016/j.pep.2005.09.003
[22] Folly-Klan M, Alix E, Stalder D, et al. A novel membrane sensor controls the localization and ArfGEF activity of bacterial RalF. PLOS Pathog. 2013;9(11): e1003747. doi: 10.1371/journal.ppat.1003747
[23] Nagai H, Roy CR. The dota protein from *Legionella pneumophila* is secreted by a novel process that requires the Dot/Icm transporter. Embo J. 2001;20 (21):5962–5970. doi: 10.1093/emboj/20.21.5962
[24] Machtens DA, Willerding JM, Eschenburg S, et al. Crystal structure of the N-terminal domain of the effector protein SidI of *Legionella pneumophila* reveals a glucosyl transferase domain. Biochem Biophys Res Commun. 2023;661:50–55. doi: 10.1016/j.bbrc.2023.04.029
[25] Tropea JE, Cherry S, Waugh DS. Expression and purification of soluble His(6)-tagged TEV protease. Methods Mol Biol. 2009;498:297–307. doi: 10.1007/978-1-59745-196-3_19
[26] Studier FW. Protein production by auto-induction in high density shaking cultures. Protein Expr Purif. 2005;41(1):207–234. doi: 10.1016/j.pep.2005.01.016
[27] Kabsch W. Integration, scaling, space-group assignment and post-refinement. Acta Crystallogr D Biol Crystallogr. 2010;66(2):133–144. doi: 10.1107/S0907444909047374
[28] Kabsch W. XDS. Acta Crystallogr D Biol Crystallogr. 2010;66(2):125–132. doi: 10.1107/S0907444909047337
[29] Skubak P, Pannu NS. Automatic protein structure solution from weak X-ray data. Nat Commun. 2013;4 (1):2777. doi: 10.1038/ncomms3777
[30] Liebschner D, Afonine PV, Baker ML, et al. Macromolecular structure determination using X-rays, neutrons and electrons: recent developments in Phenix. Acta Crystallographica Section D Struct Biol. 2019;75 (10):861–877. doi: 10.1107/S2059798319011471
[31] Emsley P, Lohkamp B, Scott WG, et al. Features and development of coot. Acta Crystallogr D Biol Crystallogr. 2010;66(4):486–501. doi: 10.1107/S0907444910007493
[32] Wernimont A, Edwards A. In situ proteolysis to generate crystals for structure determination: an update. PLOS ONE. 2009;4(4):e5094. doi: 10.1371/journal.pone.0005094
[33] Li J, Mahajan A, Tsai M-D. Ankyrin repeat: a unique motif mediating protein-protein interactions. Biochemistry. 2006;45(51):15168–15178. doi: 10.1021/bi062188q
[34] Krissinel E, Henrick K. Secondary-structure matching (SSM), a new tool for fast protein structure alignment in three dimensions. Acta Crystallographica Section D Biol Crystallogr. 2004;60(12):2256–2268. doi: 10.1107/S0907444904026460
[35] Langdon QK, Peris D, Kyle B, et al. Spplder: a species identification tool to investigate hybrid genomes with high-throughput sequencing. Mol Biol Evol. 2018;35:2835–2849. doi: 10.1093/molbev/msy166
[36] Solomon JM, Isberg RR. Growth of *Legionella pneumophila* in *Dictyostelium discoideum*: a novel system for genetic analysis of host-pathogen interactions. Trends Microbiol. 2000;8(10):478–480. doi: 10.1016/s0966-842x(00)01852-7
[37] Hägele S, Köhler R, Merkert H, et al. *Dictyostelium discoideum*: a new host model system for intracellular pathogens of the genus *Legionella*. Cell Microbiol. 2000;2 (2):165–171. doi: 10.1046/j.1462-5822.2000.00044.x
[38] Boamah DK, Zhou G, Ensminger AW, et al. From many hosts, one accidental pathogen: the diverse protozoan hosts of *Legionella*. Front Cell Infect Microbiol. 2017;7:477. doi: 10.3389/fcimb.2017.00477

[39] Park JM, Ghosh S, O'Connor TJ. Combinatorial selection in amoebal hosts drives the evolution of the human pathogen *Legionella pneumophila*. Nat Microbiol. 2020;5(4):599–609. doi: 10.1038/s41564-019-0663-7

[40] Black MH, Osinski A, Gradowski M, et al. Bacterial pseudokinase catalyzes protein polyglutamylation to inhibit the SidE-family ubiquitin ligases. Science. 2019;364(6442):787–792. doi: 10.1126/science.aaw7446

[41] Ingmundson A, Delprato A, Lambright DG, et al. *Legionella pneumophila* proteins that regulate Rab1 membrane cycling. Nature. 2007;450(7168):365–369. doi: 10.1038/nature06336

[42] Ham H, Orth K. De-AMPylation unmasked: modulation of host membrane trafficking. Sci Signal. 2011;4 (194):pe42. doi: 10.1126/scisignal.2002458

[43] Iyer S, Das C. The unity of opposites: strategic interplay between bacterial effectors to regulate cellular homeostasis. J Biol Chem. 2021;297(6):101340. doi: 10.1016/j.jbc.2021.101340

[44] Elez K, Bonvin AMJJ, Vangone A. Distinguishing crystallographic from biological interfaces in protein complexes: role of intermolecular contacts and energetics for classification. BMC Bioinf. 2018;19(S15):438. doi: 10.1186/s12859-018-2414-9

[45] Fontana MF, Banga S, Barry KC, et al. Secreted bacterial effectors that inhibit host protein synthesis are critical for induction of the innate immune response to virulent *Legionella pneumophila*. PLOS Pathog. 2011;7 (2):e1001289. doi: 10.1371/journal.ppat.1001289

[46] Belyi Y. Targeting eukaryotic mRNA translation by *Legionella pneumophila*. Front Mol Biosci. 2020;7:80. doi: 10.3389/fmolb.2020.00080

[47] De Leon JA, Qiu J, Nicolai CJ, et al. Positive and negative regulation of the master metabolic regulator mTORC1 by two families of *Legionella pneumophila* effectors. Cell Rep. 2017;21(8):2031–2038. doi: 10.1016/j.celrep.2017.10.088

[48] McCloskey A, Perri K, Chen T, et al. The metaeffector MesI regulates the activity of the *Legionella* effector SidI through direct protein–protein interactions. Microbes Infect. 2021;23(4–5):104794. doi: 10.1016/j.micinf.2021.104794

[49] Fu J, Li S, Guan H, et al. *Legionella* maintains host cell ubiquitin homeostasis by effectors with unique catalytic mechanisms. Nat Commun. 2024;15(1):5953. doi: 10.1038/s41467-024-50311-2

[50] Chauhan D, Joseph AM, Shames SR. Intrabacterial regulation of a cytotoxic effector by its cognate metaeffector promotes *Legionella pneumophila* virulence. Virulence mSphere. 2023;8(1):e0055222. doi: 10.1128/msphere.00552-22

[51] Gross SR, Kinzy TG. Improper organization of the actin cytoskeleton affects protein synthesis at initiation. Mol Cell Biol. 2007;27(5):1974–1989. doi: 10.1128/MCB.00832-06

[52] Kim S, Coulombe PA. Emerging role for the cytoskeleton as an organizer and regulator of translation. Nat Rev Mol Cell Biol. 2010;11(1):75–81. doi: 10.1038/nrm2818

[53] Lenk R, Ransom L, Kaufmann Y, et al. A cytoskeletal structure with associated polyribosomes obtained from HeLa cells. Cell. 1977;10(1):67–78. doi: 10.1016/0092-8674(77)90141-6

[54] Kaminska M, Havrylenko S, Decottignies P, et al. Dynamic organization of aminoacyl-tRNA synthetase complexes in the cytoplasm of human cells. J Biol Chem. 2009;284(20):13746–13754. doi: 10.1074/jbc.M900480200

[55] Stapulionis R, Kolli S, Deutscher MP. Efficient mammalian protein synthesis requires an intact F-actin system. J Biol Chem. 1997;272(40):24980–24986. doi: 10.1074/jbc.272.40.24980

[56] Wang T, Song X, Tan J, et al. *Legionella* effector LnaB is a phosphoryl-AMPylase that impairs phosphosignalling. Nature. 2024;631(8020):393–401. doi: 10.1038/s41586-024-07573-z

[57] Chen T-T, Lu Q, Zheng S-R, et al. Structure and mechanism of an actin-dependent bacterial phosphoryl AMPylase. Nat Chem Biol. 2025;22(1):152–162. doi: 10.1038/s41589-025-01945-w